Chemical Engineering Journal 218 (2013) 183–190

Contents lists available at SciVerse ScienceDirect

Chemical Engineering Journal

journal homepage: www.elsevier.com/locate/cej

Photocatalytic degradation of 2,4,6-trichlorophenol over g-C_3N_4 under visible light irradiation

Huanhuan Ji [a,b], Fei Chang [c], Xuefeng Hu [a,*], Wei Qin [a], Jiaowen Shen [d]

[a] Key Laboratory of Coastal Zone Environmental Processes, Yantai Institute of Coastal Zone Research, Chinese Academy of Sciences, Yantai Shandong 264003, PR China
[b] University of Chinese Academy of Science, Beijing 100049, PR China
[c] School of Environment and Architecture, University of Shanghai for Science and Technology, Shanghai 200093, PR China
[d] School of Urban Development and Environmental Engineering, Shanghai Second Polytechnic University, Shanghai 201209, PR China

HIGHLIGHTS

- g-C_3N_4 was synthesized by directly thermal condensation of dicyandiamide.
- 2,4,6-TCP could be degraded over g-C_3N_4 under visible irradiation.
- $\cdot O_2^-/\cdot OOH$ was the most important reactive species in the presence of O_2.
- 2,4,6-TCP was oxidized by hole at N_2 gas ambient in the presence of metal ions.
- The possible degradation pathway of 2,4,6-TCP was proposed.

GRAPHICAL ABSTRACT

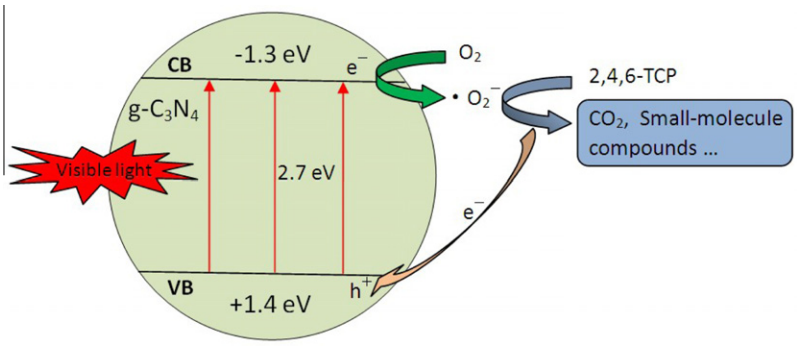

ARTICLE INFO

Article history:
Received 24 August 2012
Received in revised form 7 December 2012
Accepted 8 December 2012
Available online 27 December 2012

Keywords:
C_3N_4
Photocatalysis
2,4,6-TCP
Superoxide radical
VB holes

ABSTRACT

Graphitic carbon nitride (g-C_3N_4) was synthesized by directly thermal condensation of dicyandiamide and characterized by XRD, XPS, SEM, TEM and FT-IR. Then the as-prepared catalyst was employed to degrade priority pollutant 2,4,6-trichlorophenol (2,4,6-TCP) under visible light irradiation ($\lambda > 420$ nm). The 2,4,6-TCP could be completely mineralized over g-C_3N_4, and the pseudo-first-order rate constant for 10^{-4} M 2,4,6-TCP degradation was 0.70 h^{-1} in the presence of 1 g/L catalyst. $\cdot O_2^-/\cdot OOH$ was identified as the most important reactive species contributing to 2,4,6-TCP degradation in air. Meanwhile, valence band holes (VB holes) of g-C_3N_4 was observed to play important roles for the degradation of 2,4,6-TCP at N_2 gas ambient when metal ions were added as electron acceptors. The possible degradation pathway of 2,4,6-TCP was proposed.

1. Introduction

There is an increasing concern about g-C_3N_4 in the field of photocatalysis due to the appropriate band gap for visible light driven, reliable chemical inertness and stability. Many works based on organic dye degradation, like rhodamine B (RhB) [1], methyl orange [2], and methylene blue [3], have been devoted to study the photocatalytic performance of a variety of graphitic carbon nitrides. However, there are few reports about the photocatalytic degradation of organic pollutants by g-C_3N_4 except dyes. Very recently, mesoporous g-C_3N_4 was employed to treat 4-chlorophenol and phenol in water by Wang et al. [4]. But the porous g-C_3N_4 involved complex synthetic procedure and template using. In their research, the bulk g-C_3N_4 prepared by ammonium thiocyanate showed very low photocatalytic activity. For the wide application of the graphitic carbon nitride catalysts, it is urgent to investigate their performances in catalyzing the photodegradation of various pollutants.

* Corresponding author. Tel.: +86 535 2109157; fax: +86 535 2109000.
E-mail address: xfhu@yic.ac.cn (X. Hu).

1385-8947/$ - see front matter © 2012 Elsevier B.V. All rights reserved.
http://dx.doi.org/10.1016/j.cej.2012.12.033

The g-C_3N_4 has shown a distinct photocatalytic mechanism in the previous studies because of its unique positions of the conduction band (CB) and valence band (VB) (CB = −1.3 V, VB = 1.4 V *vs.* NHE, pH = 7) [5,6]. Wang et al. thought that the degradation of organic pollutants over the g-C_3N_4 was mainly attributed to reactive oxygen species produced by photogenerated electrons [4], and the role of VB holes was not mentioned. However, Yan et al. [1] reported that the degradation of RhB over g-C_3N_4 mainly originated from the photogenerated holes oxidation. As a new-type photocatalyst, the real oxidative species for organic degradation still remains elusive. So it is important to investigate the catalytic mechanism of g-C_3N_4, especially the pure g-C_3N_4 under different conditions during various environmental pollutants photodegradation.

Chlorophenols (CPs) are common and recalcitrant environmental pollutants. Because of the high toxicity, carcinogenic properties, and bioaccumulation capability, four of the chlorophenols (2-CP, 2,4-DCP, 2,4,6-TCP, and PCP) have been classified as priority pollutants by the U.S. Environmental Protection Agency (EPA) [7]. 2,4,6-TCP is one of the most significant pollutants among CPs and is often used to test the efficiency of oxidation methods [8]. Several strategies have been followed to remove CPs from the environment. Conventional methods include thermal, chemical and biological treatments, which, however, were restricted by toxic by-product generation, incomplete mineralization or specific conditions [9,10]. Heterogeneous photocatalysis technique is one of the most promising candidates to completely destroy CPs. In addition, this process allows the efficient degradation of a variety of organic pollutants at low concentration levels in aqueous wastes [11].

In this work, the pure g-C_3N_4 was synthesized by directly thermal condensation of dicyandiamide, and was employed to decompose 2,4,6-TCP under the irradiation of visible light ($\lambda > 420$ nm). The photocatalytic degradation mechanism of 2,4,6-TCP in aqueous dispersed g-C_3N_4 was discussed systematically. The roles of reactive oxygen species produced during the photocatalysis process were evaluated. $\cdot O_2^-$/·OOH was the most important reactive species contributing to 2,4,6-TCP degradation in air. **.**OH derived from $\cdot O_2^-$/·OOH also play a role for 2,4,6-TCP degradation. Photogenerated holes show the ability to oxidize 2,4,6-TCP directly, which was verified by using metal ions as the electron acceptor under N_2 gas ambient.

2. Experimental

2.1. Reagents and solutions

Dicyandiamide (>98.0%) was purchased from Tokyo Chemical Industry CO., Ltd. (Tokyo, Japan). 2,4,6-Trichlorophenol (2,4,6-TCP) (98%) was purchased from Aladdin Chemistry CO., Ltd. (Shanghai, China). 1,4-Benzoquinone (97%), dehydrated alcohol (99.7%), EDTA–Na_2 (⩾99.0%), NaN_3 and triethanolamine (TEOA) (A.R.) were used as additives. N,N-Diethyl-*p*-phenylenediamine (DPD) (98%), Peroxidase (POD) [from horseradish, 200 units/mg] were purchased from J&K Scientific Ltd. (Beijing, China). $PbCl_2$ (⩾99.0%), $NiCl_2{\cdot}6H_2O$ (⩾98.0%), $HgCl_2$ (⩾99.5%), $Cu(NO_3)_2{\cdot}3H_2O$ (⩾99.0%), $CdCl_2{\cdot}2.5H_2O$ (⩾99.0%), $K_2Cr_2O_7$ (>99.8%) were all analytical reagents. All reagents were used as received without further purification. Aqueous solutions were prepared with freshly deionized water (18.2 MΩ cm specific resistance) by a Pall Cascada laboratory water system.

2.2. Synthesis and characterization of g-C_3N_4

A 50 mL ceramic crucible containing 2 g dicyandiamide was introduced into a muffle furnace. Within 4 h, the temperature of the furnace raised to 550 °C from room temperature. The dicyandiamide was calcined at this temperature for 4 h and then cooled to room temperature before removing from the furnace. The obtained yellow products were collected and ground into powder prior to use.

The crystal structure of the samples was investigated using X-ray diffraction (XRD; Rigaka D/max 2500 X-ray diffractometer) with Cu Kα_1 radiation, $\lambda = 1.54056$ Å. X-ray photoelectron spectroscopy (XPS) data were obtained with an ESCALab220i-XL electron spectrometer from VG Scientific using 300 W Al Kα radiation. The binding energies were referenced to the C 1s line at 284.8 eV from adventitious carbon. The morphology of the samples was examined by field emission scanning electron microscopy (SEM; Hitachi S-4800) and transmission electron microscopy (TEM; JEOL JEM-1400). The Fourier transform infrared (FT-IR) spectrum of the sample was recorded on a Nicolet iS 10 FT-IR spectrometer.

2.3. Photocatalytic degradation of 2,4,6-TCP

A 300 W Xe lamp was used as the light source and a cut-off filter was used to ensure irradiation by the light above 420 nm. In a typical reaction, 20 mL solution with 20 mg catalyst was injected into a 50 mL quartz bottle. The mixture was magnetically stirred for 0.5 h under dark to obtain adsorption/desorption equilibrium of 2,4,6-TCP on the catalyst. The solution was then exposed to visible light. At irradiation time intervals of every 0.5 h, 2 mL sample was collected from the mixture, centrifuged at 4000 rpm for 10 min to remove the catalyst, and then filtered through a 0.22 μm filter membrane before HPLC analysis.

When the reaction was conducted at N_2 gas ambient, the quartz bottle was sealed with Teflon-lined rubber septa and aluminum crimp caps. N_2 gas was purged into the bottle through a Teflon tube during the whole reaction.

2.4. Analyses

The concentration of 2,4,6-TCP was measured by a HPLC (waters 2695–2998) system installed with a Sun Fire™ C18 (5 μm, 4.6 × 250 mm) reversed phase column at 30 °C. Separation of degradation intermediates was realized by using an eluent composed of methanol and 1% (v/v) acetic acid in water (70/30 v/v) at a flow rate of 1.0 mL/min. For liquid chromatography/mass spectrometry (LC–MS) detection, 40 mL 5×10^{-4} M 2,4,6-TCP solution was used. When a portion of 2,4,6-TCP was degraded (ca. 70%), the solution was centrifuged and filtered. Then the sample was concentrated into 1 mL methanol solution using a waters Oasis HLB solid phase extraction (SPE) column. MS experiments were achieved on a Finnigan LCQ (San José, CA, USA) ion trap mass spectrometer using negative and positive electrospray as the ionization processes. The electron spin resonance (ESR) signals of radicals spin trapped by DMPO were detected at ambient temperature on a Bruker (ESP 300E) spectrometer. For H_2O_2 concentration analysis, 1 ml sample, 1 ml pH 6.0 buffer, 50 μL DPD and 50 μL POD were mixed in a 1 cm cuvette. The absorption spectrum was measured after 45 s reaction by a spectrophotometer (Beckman coulter DU800). Preparation of pH buffer, DPD and POD solution, as well as the calculation of H_2O_2 concentration were performed according to literature [12]. The total organic carbon (TOC) values along with 2,4,6-TCP degradation were determined using a TOC auto analyzer (Shimadzu TOC-VCPH, Japan). The release of chloride ions was monitored using an ion chromatograph (Dionex ICS3000). The buffer solution was 4.5 mM Na_2CO_3/0.8 mM $NaHCO_3$, and a Dionex AS18 column was used.

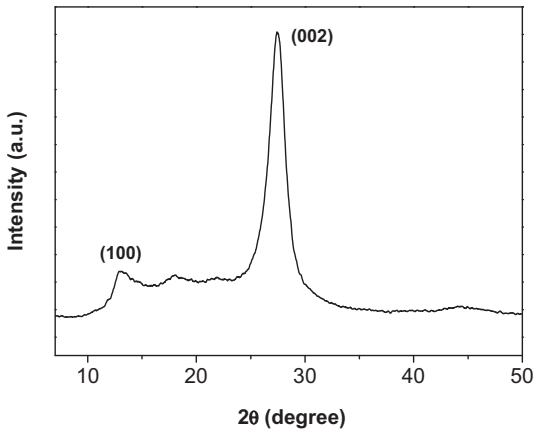

Fig. 1. XRD pattern for the as-prepared g-C_3N_4.

3. Results and discussion

3.1. Physicochemical properties of the as-prepared g-C_3N_4

Fig. 1 shows the XRD pattern of the as-prepared g-C_3N_4, a typical g-C_3N_4 structure is suggested by two obvious peaks. The strongest peak at 27.42 is a characteristic interlayer stacking peak of aromatic systems, indexed as the (002) plane for graphitic materials [1]. The calculated interplanar distance of aromatic units is d = 0.325 nm. The relatively weak peak at 13.14, which corresponds to a distance d = 0.685 nm and is indexed as (100) plane, is associated with an in-plane structural packing motif.

Fig. 2 shows the XPS spectra of g-C_3N_4 synthesized by thermal condensation of dicyandiamide precursor. The peaks at 288, 399 and 533 eV in the survey spectrum were due to photoelectrons excited from the C 1s, N 1s and O 1s levels respectively. In C 1s higher resolution spectrum, the two features of binding energy values can be attributed to sp^2-hybridized carbon in the aromatic ring (287.8 eV) [13], and a carbon-containing contamination (284.8 eV) [14]. The N 1s spectrum in Fig. 2c was deconvoluted into four peaks. The peak centered at 398.2 eV is attributable to sp^2 N involved in triazine rings, whereas the contribution at 398.8 eV corresponds to bridged nitrogen atoms N–$(C)_3$. The peak at the position of 400.8 eV may be attributed to the $-NH_2$ or = NH groups [15]. Charging effects or positive charge localization in heterocycles can lead to the peak at 404.6 eV [13]. In O 1s XPS spectrum, the peak at the position of 532.5 eV was attributed to surface –OH groups derived from surface oxygen contaminates [16].

The Fourier transform infrared (FT-IR) result proves the existence of a graphite-like structure of carbon nitride again as shown in Fig. 3. The broadband at 3100–3300 cm^{-1} can be assigned to the stretching modes of secondary and primary amines and their intermolecular hydrogen-bonding interactions. The stretching vibration of O–H is also contributed to the broad absorption in this region [17]. Several strong bands in the 1200–650 cm^{-1} region correspond to the typical stretching modes of CN heterocycles [18]. Additionally, the characteristic ring breath of the triazine units is found at 809 cm^{-1} [19].

The morphology and microstructure of the bulk g-C_3N_4 sample were revealed by SEM and TEM, as shown in Fig. 4. The powder sample appears to have agglomeration structures on the SEM micrograph image. TEM image directly reflects the inner structure

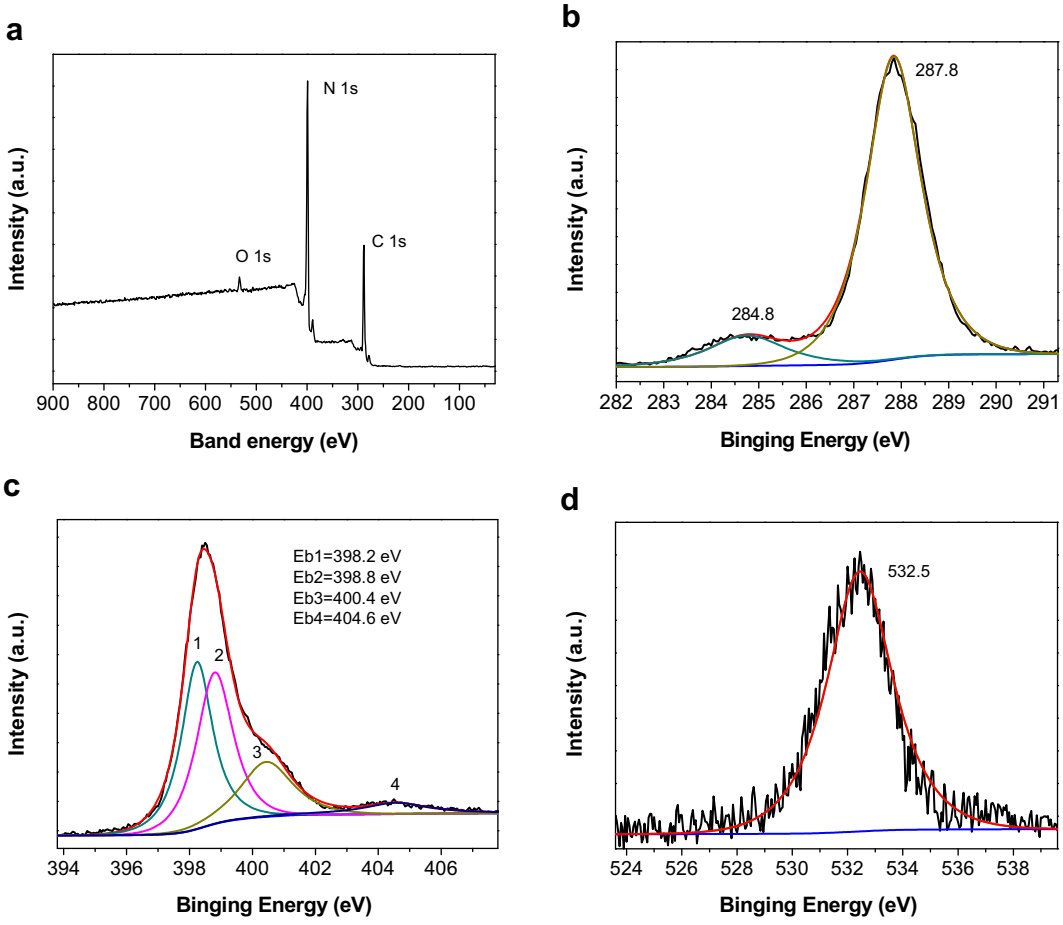

Fig. 2. XPS survey spectrum of the as-prepared g-C_3N_4 (a) and the corresponding high-resolution XPS spectra of C 1s (b) N 1s (c) and O 1s (d).

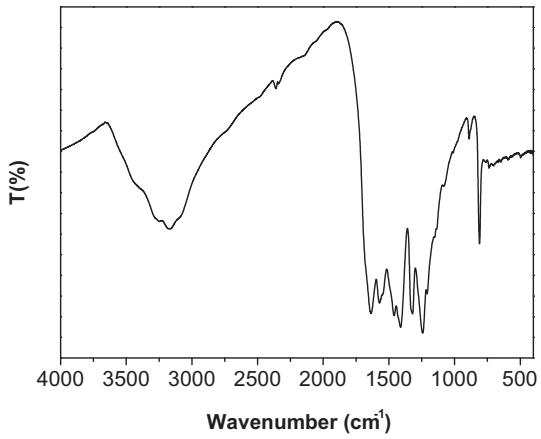

Fig. 3. FT-IR spectrum for the as-prepared g-C_3N_4.

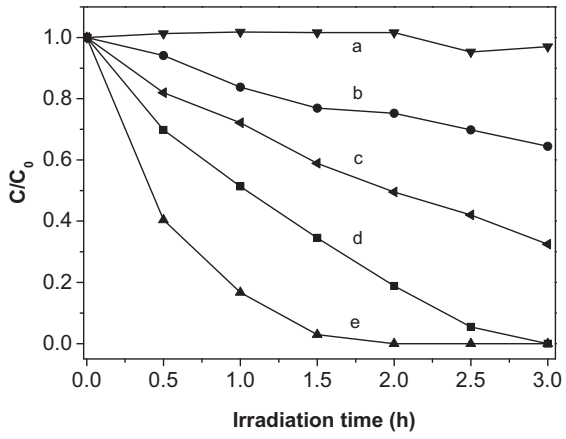

Fig. 5. Visible light degradation of 2,4,6-TCP in the absence (a) or presence (b–e) of g-C_3N_4. Initial concentration of 2,4,6-TCP: 10^{-4} M (a); 5×10^{-4} M (b); 2×10^{-4} M (c); 10^{-4} M (d); 5×10^{-5} M (e).

of the g-C_3N_4 sample [13]. Some irregular strips and sheet structures are observed in the image.

3.2. Photocatalytic performance

The photocatalytic activity of the as-prepared g-C_3N_4 was evaluated by the degradation of 2,4,6-TCP under visible light, as shown in Fig. 5. The concentration of 10^{-4} M 2,4,6-TCP solution exhibited no obvious degradation after 3 h visible light irradiation in the absence of catalyst (curve a). In contrast, the same concentration of 2,4,6-TCP was efficiently degraded in the presence of 1 g/L g-C_3N_4 under the identical condition (curve d). The degradation values after 3 h for different initial 2,4,6-TCP concentrations are listed in Table 1.

The degradations of different initial concentration of 2,4,6-TCP catalyzed by g-C_3N_4 under the irradiation of visible light were described by pseudo-first-order rate equation (Eq. (1)) [20,21]:

$$\ln(C/C_0) = -kt \quad (1)$$

The linearity of $\ln(C/C_0)$ *vs.* t is quite well at a specific concentration, although the concentration-dependence of rate constant suggests that the photodegradation of 2,4,6-TCP is not really first order reaction. This is quite common in the photocatalytic degradation studies for many other organic compounds in a dilute solution [22]. The rate constants (k) were determined from the linear relationship of $\ln(C/C_0)$ *vs.* reaction time. Because of the formation of intermediates, the reactions may not well follow the equation in the final stage. The pseudo-first-order rate constants and related coefficients for different initial concentrations of 2,4,6-TCP degradation are shown in Table 1. When the initial concentration of 2,4,6-TCP increased from 5×10^{-5} M to 10^{-3} M, the amount of destroyed 2,4,6-TCP increased from 5×10^{-5} to 1.78×10^{-4} M, but the rate constant (k) decreased from 1.79 to 0.14.

Table 1
The parameters for different initial concentrations of 2,4,6-TCP degradation.

Initial 2,4,6-TCP concentration (M)	5×10^{-5}	10^{-4}	2×10^{-4}	5×10^{-4}
Degradation amount in 3 h (M)	5×10^{-5} [a]	10^{-4}	1.35×10^{-4}	1.78×10^{-4}
Rate constant (h^{-1})	1.79	0.70	0.35	0.14
Related coefficient	0.9999	0.9967	0.9973	0.9782

[a] The 5×10^{-5} M 2,4,6-TCP was already completely degraded after 2 h reaction.

Photocatalysis is usually considered as diffusion controlled reaction. As the 2,4,6-TCP initial concentration increased, the degradation reaction would accelerate, because the diffusion is accelerated. This means a larger amount of 2,4,6-TCP degraded in the same reaction time. On the other hand, photocatalysis occur through a series of consecutive reactions, the formation, migration and reaction of photogenerated radicals with organic compounds. Any of these processes could determine the overall degradation rate [20]. When increased the initial concentration, a bigger quantity of 2,4,6-TCP would adsorb on the surface of g-C_3N_4, meanwhile the active sites left for generating active species would be reduced. Furthermore, as more 2,4,6-TCP degraded, more intermediates generated in the reaction system. These intermediates would compete with 2,4,6-TCP for active species and active sites. This re-

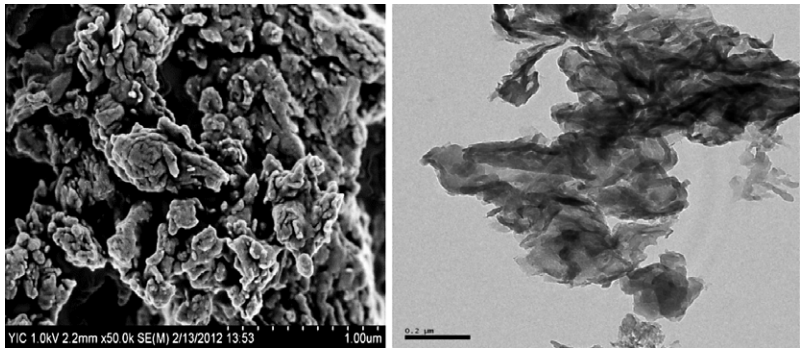

Fig. 4. SEM (left) and TEM (right) images for the as-prepared g-C_3N_4.

sults in the rate constant decrease with increasing initial concentration.

3.3. Catalytic degradation mechanism

The mechanism of g-C_3N_4 photocatalytic degradation of 2,4,6-TCP was investigated by a set of experiments (Fig. 6). N_2 gas was used to expel dissolved oxygen in the solution and maintain an anaerobic environment. Other additives acted as active species scavengers were used to assess the contribution of the corresponding active species in the system.

As shown in Fig. 6, the degradation was greatly suppressed in N_2 gas ambient. This phenomenon implied that dissolved oxygen played a crucial role in the g-C_3N_4 photocatalysis process. According to literatures [23,24], the molecular O_2 can efficiently scavenge photogenerated electrons forming superoxide radical ($\cdot O_2^-$). Then superoxide radical could react with proton to produce hydroperoxide radical (**.**OOH) (Eqs. (2), (3)):

$$O_2 + e^- \rightarrow \cdot O_2^- \quad (2)$$

$$O_2^- + H^+ \rightarrow \cdot OOH \quad (3)$$

ESR technology was used to confirm the generation of $\cdot O_2^-$. There was no signal in dark, however, characteristic peaks of DMPO – $\cdot O_2^-/\cdot OOH$ adducts ($g = 2.0063$) emerged and increased with time when irradiated with visible light, as seen from Fig. 7.

The role of the $\cdot O_2^-/\cdot OOH$ was evaluated by adding its scavenger, 1,4-benzoquinone, to the reaction system. Degradation rate of 2,4,6-TCP in air in the presence of 1,4-benzoquinone is close to that at N_2 gas ambient (Fig. 6). It was presumed that $\cdot O_2^-/\cdot OOH$ or other active species derived from it were involved in the degradation of 2,4,6-TCP degradation.

In addition to superoxide radical, singlet oxygen ($^1O_2$) was also possible oxidative species. The addition of NaN_3 as a scavenger for $^1O_2$ suppressed the degradation of 2,4,6-TCP slightly (Fig. 6), $^1O_2$ is unlikely to be a significant active specie.

Hydroxyl radicals (·OH) is another important reactive oxygen species, possessing a more positive oxidative capacity than $\cdot O_2^-$. As the VB potential energy of g-C_3N_4 is 1.4 V, the VB holes are incapable of directly oxidizing the surface hydroxyl groups or adsorbed water molecules to generate ·OH ($E^0(\cdot OH/OH^-_{surf}) = 1.9$ V, $E^0(\cdot OH/H_2O_{ads}) = 2.7$ V *vs.* NHE) [5,25]. When ·OH scavenger (ethanol) was added, the degradation of 2,4,6-TCP was similar to the simple 2,4,6-TCP/g-C_3N_4 system at the initial stage but slower at the following stage (Fig. 6). Thus a small amount of the hydroxyl radicals (·OH) may be produced in the catalysis process. The

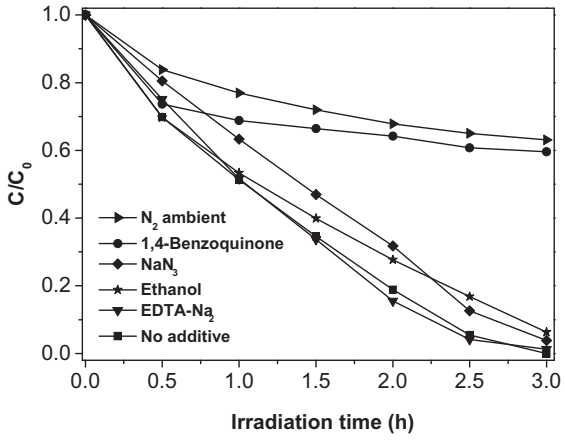

Fig. 6. Photocatalytic degradation of 2,4,6-TCP with various radical scavenger additives (10^{-4} M 2,4,6-TCP, 1 g/L g-C_3N_4, additive concentration is 10^{-2} M).

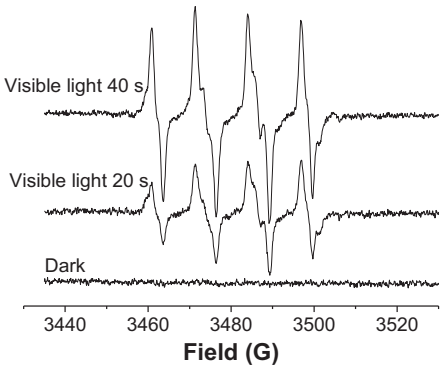

Fig. 7. ESR spectra of DMPO – $\cdot O_2^-/\cdot OOH$ adducts in the system of g-C_3N_4 before and after visible light (532 nm) irradiation.

formation of ·OH can be expected on the basis of the equations (Eqs. (4)–(6)):

$$\cdot O_2^- + e^- + 2H^+ \rightarrow H_2O_2 \quad (4)$$

$$\cdot OOH + e^- + H^+ \rightarrow H_2O_2 \quad (5)$$

$$H_2O_2 + e^- \rightarrow \cdot OH + OH^- \quad (6)$$

The formation of hydrogen peroxide (H_2O_2) was checked by a modified spectrophotometric analysis method according to Bader et al. [12]. As shown in Fig. 8, the concentration of H_2O_2 increased continuously and quickly. It reached to 38 μM after a 3 h reaction. The high concentration of H_2O_2 contributed to the rapid and complete degradation of 2,4,6-TCP.

The generation of ·OH was also confirmed by ESR technique (Fig. 9). Along with irradiation time, the weak DMPO–·OH signals ($g = 2.0063$) were emerged gradually. Using the stack method, the characteristic peaks with an intensity ratio of 1:2:2:1 could be verified.

Generally, the photodegradation activity of semiconductor photocatalyst originates from photogenerated holes in valence band and photogenerated electrons in conduction band. VB holes are also oxidative species and may directly cause the organic pollutant degradation. EDTA–Na_2, an efficient holes scavenger, was employed to discern the contribution of g-C_3N_4 VB holes in 2,4,6-TCP degradation. In Fig. 6, the curve almost overlaps with the curve of no additive reaction. Actually, oxalate and triethanolamine (TEOA) were also employed as hole scavengers (given in the Supporting Information Part 1), and the results are similar with EDTA-Na_2 experiment. Although about 15% 2,4,6-TCP is still in the solution after 3 h reaction in the TEOA experiment, the proportion is small compared with the experiment of 1,4-benzoquinone as $\cdot O_2^-$ scavenger (about 60% left). The slight effect of TEOA may stem from that 2,4,6-TCP diffusion in the solution and adsorption on g-C_3N_4 surface were suppressed by high concentration of TEOA (10 vol.%). These results illustrate that g-C_3N_4 VB holes do not show effect on the photocatalysis reaction rate in the 2,4,6-TCP/g-C_3N_4 system at the natural condition. In other words, 2,4,6-TCP oxidative degradation originated mainly from g-C_3N_4 photogenerated electrons but not the holes in the presence of oxygen. It also reveals that $\cdot O_2^-/\cdot OOH$ is the dominant active species in the reaction system in the presence of molecular oxygen. Nevertheless, since VB holes need accept electrons to restore the original state for preparing next excitation, it was speculated that excess electrons were released during 2,4,6-TCP photodegradation. Thus, VB holes would contribute to the organic pollutants transformation through the process of obtaining electrons from the intermediates, radials and even very little 2,4,6-TCP.

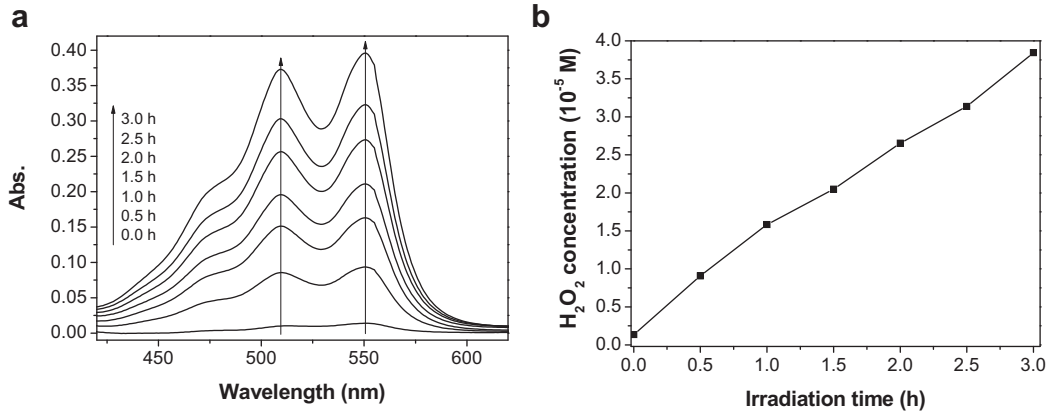

Fig. 8. H_2O_2 formation during irradiating the mixture of 2,4,6-TCP and g-C_3N_4 with visible light: spectral evolution (a) and H_2O_2 concentration verse time (b).

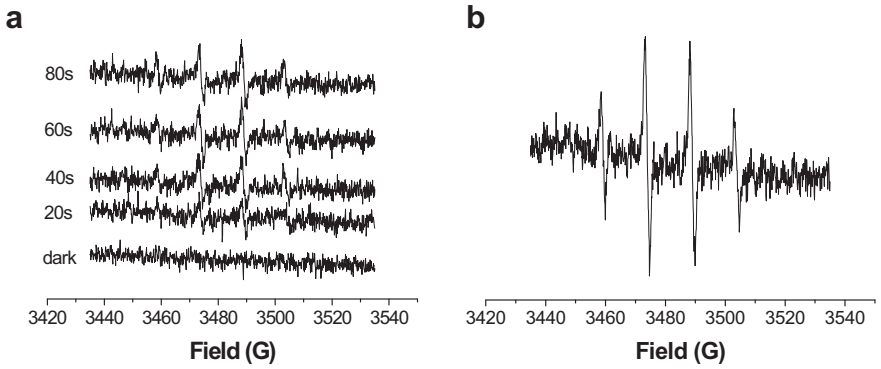

Fig. 9. ESR spectra of DMPO–·OH adducts in the system of g-C_3N_4 before and after visible light (532 nm) irradiation (a), and stack of visible light irradiation result (b).

3.4. Metal ions act as electrons scavengers

To make clear if VB holes can oxidize organic compounds such as 2,4,6-TCP directly, oxygen was removed from the reaction system. Besides molecular oxygen, any dissolved species with a reduction potential more positive than the conduction band of the photocatalyst can, in principle, consume electrons [26]. The g-C_3N_4 possesses a conduction band (CB) of -1.3 V, so it is capable of reducing most metal ions such as $Cr_2O_7^{2-}$, Hg^{2+}, Cu^{2+}, Pb^{2+}, Ni^{2+}, Cd^{2+}, Zn^{2+} theoretically.

2,4,6-TCP photocatalytic degradation in the presence of metal ions was investigated by adding corresponding metal salts to the reaction system at N_2 gas ambient (Fig. 10). The 2,4,6-TCP degradation is prominent compared with no metal additives in the absence of oxygen. Metal ions and the reduced metals clearly don't possess the ability of degrading organic compounds. At N_2 gas ambient, hole scavenger TEOA was added in the Cd^{2+}/2,4,6-TCP/g-C_3N_4 reaction system and the 2,4,6-TCP degradations were greatly suppressed. The curve is comparative with no metal ions reaction. Therefore, the experiment at N_2 ambient well demonstrated that 2,4,6-TCP could be oxidative degradation by photogenerated holes in the valence band of g-C_3N_4 after the conduction electrons were transformed.

3.5. Intermediates identification

Several researches reported that the first step of 2,4,6-TCP oxidative degradation was to generate 2,6-dichloro-1,4-benzoquinone (2,6-DCQ), a light sensitive compound easily transforming into a mixture of 2,6-dichlorohydroquinone (DCHQ) and 2,6-dichloro-3-hydroxy-1,4-benzoquinone (DCHB) under light irradiation [27]. These aromatics could be destructed *via* the aromatic ring cleavage [28]. And the final mineralized products were small molecular aliphatic carboxylic acids [29]. However, these results were obtained by FePcS/H_2O_2 [30], O_3 [31], H_2O_2/polymer [10] oxidation or catalysis oxidation, but not by oxygen oxidation.

In this work, five intermediates were detected in the process of 2,4,6-TCP photodegradation in air (shown in the Supporting Information Part 2). The generation of 2,6-DCQ was identified by comparing with authentic compound using HPLC. 2,6-DCQ was

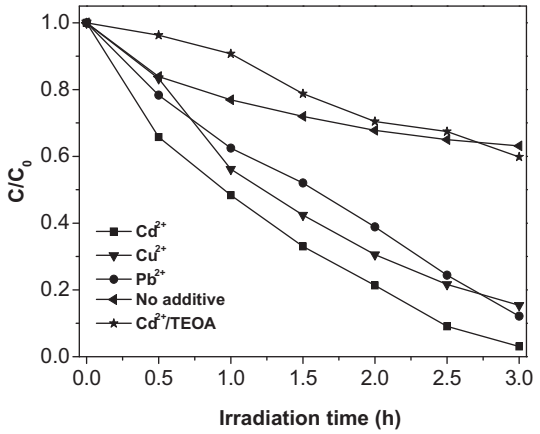

Fig. 10. 2,4,6-TCP photocatalysis degradation in metal/organic coexist system at N_2 gas ambient (2×10^{-4} M metal ions, 10^{-4} M 2,4,6-TCP, 1 g/L g-C_3N_4, 10 vol.% TEOA, pH adjusted to 5.1).

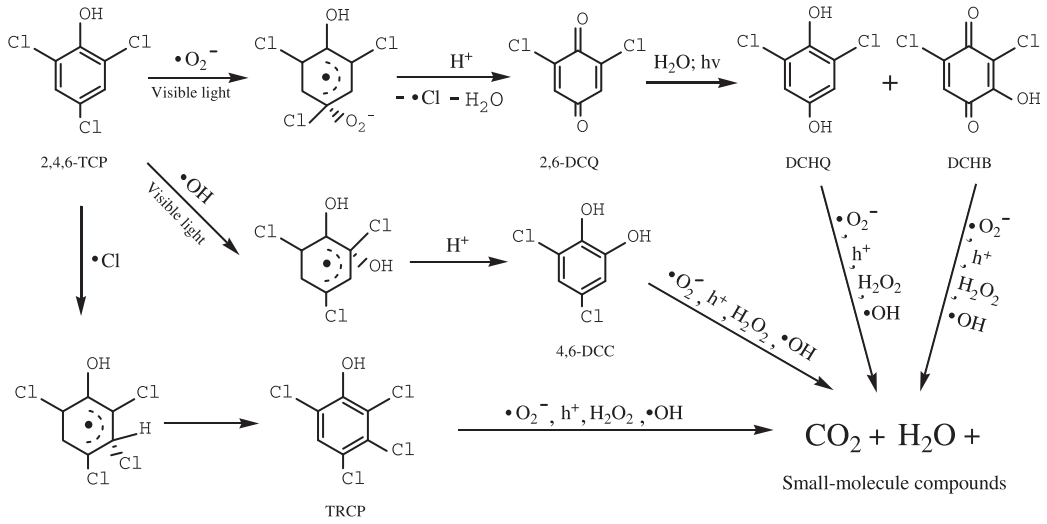

Scheme 1. The possible pathway for 2,4,6-TCP degradation.

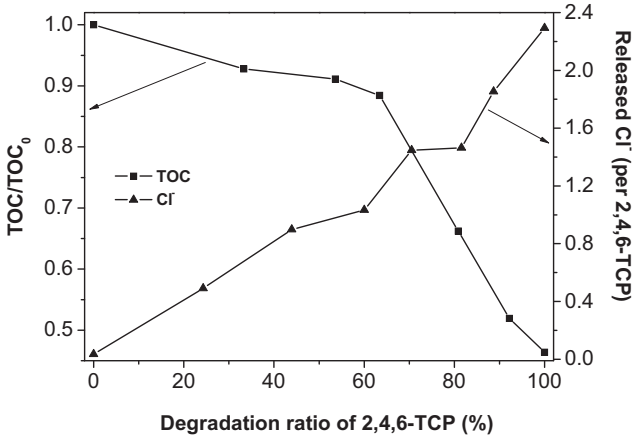

Fig. 11. TOC removal and Cl^- release during 2,4,6-TCP degradation catalyzed by g-C_3N_4 under visible light irradiation.

detected immediately after the sample was withdrawn from the reaction because of its instability under light irradiation. DCHB and 2,6-DCHQ were examined by comparing the HPLC chromatogram of 2,4,6-TCP degradation and 2,6-DCQ solution under light irradiation. A SPE-LCMS analysis method was also used to render the molecular information of DCHB and 2,6-DCHQ. Based upon the LC-MS data, two other intermediates: 4,6-dichlorocatechol (4,6-DCC) and 2,3,4,6-tetrachlorophenol (TRCP) were also detected. It is possible for ·OH from the H_2O_2 decomposition to attack 2,4,6-TCP molecules to create 4,6-DCC. TRCP may derive from the reaction between chlorine radical (·Cl, formed during dechlorination of chlorophenol) and 2,4,6-TCP.

The intermediates generated at N_2 gas ambient in the presence of Cd^{2+} ions was also checked by LC-MS (shown in the Supporting Information Part 2). DCHB and 4,6-DCC are absent and some new unidentified peaks appear in the HPLC chromatogram. This indicates that VB holes can oxidize 2,4,6-TCP directly and the formed intermediates are different from $\cdot O_2^-$ oxidation. The role of VB holes cannot be observed in the presence of oxygen may be due to (1) VB holes may also oxidize the degradation intermediates and the formed radials; (2) the strong degradation ability of $\cdot O_2^-$ overshadow the hole oxidation ability; (3) the hole was removed in hole scavenging experiments, the recombination of electron–hole was depressed and more $\cdot O_2^-$ was generated for the degradation of 2,4,6-TCP.

According to the discussion above, the possible pathway for 2,4,6-TCP degradation and intermediates generation is shown in Scheme 1.

3.6. TOC removal and Cl^- release analyses

To further verify the photocatalytic performance of g-C_3N_4, the curves of total organic carbon (TOC) removal and Cl^- release were obtained as a function of 2,4,6-TCP degradation ratio (Fig. 11).

As shown in Fig. 11, the removal of TOC was slowly at the initial stage, and then accelerated after 60% 2,4,6-TCP was degraded, which is consistent with the proposed degradation pathway. 2,4,6-TCP was oxidized by active oxygen species to generate the aromatic intermediates at the first step, which then open the aromatic ring and mineralize to CO_2 finally. When the 2,4,6-TCP was fully destroyed, above 50% TOC was removed simultaneously. In the Cl^- release curve, average 2.3 chlorine ions were released per 2,4,6-TCP molecule at the point of 2,4,6-TCP 100% degradation. This catalyst showed the good ability to carry out the deep oxidation of 2,4,6-TCP.

The stability of g-C_3N_4 was evaluated by repeating the photodegradation reaction five times under similar conditions after reisolation of the catalyst (Supporting Information Part 3). During the catalytic cycles, no activity decrease is observed. XPS measurements of the catalyst after the catalytic cycle experiments show no significant differences from freshly prepared samples (Supporting Information Part 3). The results indicated that the catalyst show good stability in photodegradation reaction.

4. Conclusion

The as-prepared g-C_3N_4 showed good capacity to mineralize priority pollutant 2,4,6-TCP under visible light irradiation. 10^{-4} M 2,4,6-TCP was destroyed after 3 h photodegradation, and above 50% TOC removal ratio was reached. At the natural ambient, $\cdot O_2^-$/·OOH was the dominant reactive oxygen species contributed to 2,4,6-TCP degradation, while 2,4,6-TCP could be degraded by VB holes in the presence of appropriate electron acceptor at N_2 gas ambient. Our results clearly indicate that g-C_3N_4 possesses a good potential in photocatalysis treatment of waste water, especially photocatalytic oxidation of organic pollutants and simultaneous reduction of metal ions to facilitate the recovery process.

Acknowledgments

The generous supports by the National Natural Science Foundation of China (No. 41076040, No. 20807036), the Yantai Science & Technology Bureau (Project 2010160) and Training Program for Young Teachers in Shanghai Colleges and Universities (egd11008) are acknowledged.

Appendix A. Supplementary material

Supplementary data associated with this article can be found, in the online version, at http://dx.doi.org/10.1016/j.cej.2012.12.033.

References

[1] S.C. Yan, Z.S. Li, Z.G. Zou, Photodegradation of rhodamine B and methyl orange over boron-doped g-C_3N_4 under visible light irradiation, Langmuir 26 (2010) 3894–3901.
[2] L. Ge, C. Han, J. Liu, Novel visible light-induced g-C_3N_4/Bi_2WO_6 composite photocatalysts for efficient degradation of methyl orange, Appl. Catal. B 108-109 (2011) 100–107.
[3] L. Song, S. Zhang, X. Wu, Q. Wei, A metal-free and graphitic carbon nitride sonocatalyst with high sonocatalytic activity for degradation methylene blue, Chem. Eng. J. 184 (2012) 256–260.
[4] Y. Cui, J. Huang, X. Fu, X. Wang, Metal-free photocatalytic degradation of 4-chlorophenol in water by mesoporous carbon nitride semiconductors, Catal. Sci. Technol. 2 (2012) 1396–1402.
[5] Y. Zheng, J. Liu, J. Liang, M. Jaroniec, S.Z. Qiao, Graphitic carbon nitride materials: controllable synthesis and applications in fuel cells and photocatalysis, Energy Environ. Sci. 5 (2012) 6717–6731.
[6] Y. Cui, Z. Ding, P. Liu, M. Antonietti, X. Fu, X. Wang, Metal-free activation of H_2O_2 by g-C_3N_4 under visible light irradiation for the degradation of organic pollutants, Phys. Chem. Chem. Phys. 14 (2012) 1455–1462.
[7] M. Jin, X. Chen, B. Pan, Simultaneous determination of 19 chlorophenols in water by liquid chromatography-mass spectrometry with solid-phase extraction, J. Liq. Chromatogr. Related Technol. 29 (2006) 1369–1380.
[8] G. Lente, J.H. Espenson, Oxidation of 2,4,6-trichlorophenol by hydrogen peroxide, comparison of different iron-based catalysts, Green Chem. 7 (2005) 28–34.
[9] M. Pera-Titus, V. García-Molina, M.A. Baños, J. Giménez, S. Esplugas, Degradation of chlorophenols by means of advanced oxidation processes: a general review, Appl. Catal. B 47 (2004) 219–256.
[10] G. Díaz-Díaz, M. Celis-García, M.C. Blanco-López, M.J. Lobo-Castañón, A.J. Miranda-Ordieres, P. Tuñón-Blanco, Heterogeneous catalytic 2,4,6-trichlorophenol degradation at hemin-acrylic copolymer, Appl. Catal. B 96 (2010) 51–56.
[11] D. Fabbri, A. Prevot, E. Pramauro, Effect of surfactant microstructures on photocatalytic degradation of phenol and chlorophenols, Appl. Catal. B 62 (2006) 21–27.
[12] H. Bader, V. Sturzenegger, J. Hoigné, Photometric method for the determination of low concentrations of hydrogen peroxide by the peroxidase catalyzed oxidation of N, N-diethyl-p-phenylenediamine (DPD), Water Res. 22 (1988) 1109–1115.
[13] Y. Cui, J. Zhang, G. Zhang, J. Huang, P. Liu, M. Antonietti, X. Wang, Synthesis of bulk and nanoporous carbon nitride polymers from ammonium thiocyanate for photocatalytic hydrogen evolution, J. Mater. Chem. 21 (2011) 13032–13039.
[14] A.P. Dementjev, A. de Graaf, M.C.M. van de Sanden, K.I. Maslakov, A.V. Naumkin, A.A. Serov, X-Ray photoelectron spectroscopy reference data for identification of the C_3N_4 phase in carbon–nitrogen films, Diamond Relat. Mater. 9 (2000) 1904–1907.
[15] Q. Guo, Y. Xie, X. Wang, S. Lv, T. Hou, X. Liu, Characterization of well-crystallized graphitic carbon nitride nanocrystallites via a benzene-thermal route at low temperatures, Chem. Phys. Lett. 380 (2003) 84–87.
[16] K.L. Purvis, G. Lu, J. Schwartz, S.L. Bernasek, Surface characterization and modification of indium tin oxide in ultrahigh vacuum, J. Am. Chem. Soc. 122 (2000) 1808–1809.
[17] B.V. Lotsch, W. Schnick, From triazines to heptazines: novel nonmetal tricyanomelaminates as precursors for graphitic carbon nitride materials, Chem. Mater. 18 (2006) 1891–1900.
[18] M.J. Bojdys, J.O. Müller, M. Antonietti, A. Thomas, Ionothermal synthesis of crystalline, condensed, graphitic carbon nitride, Chem. Eur. J. 14 (2008) 8177–8182.
[19] S.C. Yan, Z.S. Li, Z.G. Zou, Photodegradation performance of g-C_3N_4 fabricated by directly heating melamine, Langmuir 25 (2009) 10397–10401.
[20] N.A. Laoufi, D. Tassalit, F. Bentahar, The degradation of phenol in water solution by TiO_2 photocatalysis in a helical reactor, Global NEST J. 10 (2008) 404–418.
[21] D. Chen, A.K. Ray, Photodegradation kinetics of 4-nitrophenol in TiO_2 suspension, Water Res. 32 (1998) 3223–3234.
[22] Y. Xu, C.H. Langford, Variation of Langmuir adsorption constant determined for TiO_2-photocatalyzed degradation of acetophenone under different light intensity, J. Photochem. photobiol. A: Chem. 133 (2000) 67–71.
[23] E. Brillas, E. Mur, R. Sauleda, L. Sànchez, J. Peral, X. Domènech, J. Casado, Aniline mineralization by AOP's: anodic oxidation, photocatalysis, electro-Fenton and photoelectro-Fenton processes, Appl. Catal. B 16 (1998) 31–42.
[24] D. Chatterjee, S. Dasgupta, Visible light induced photocatalytic degradation of organic pollutants, J. Photochem. Photobiol. C 6 (2005) 186–205.
[25] W. Choi, Pure and modified TiO_2 photocatalysts and their environmental applications, Catal. Surv. Asia 10 (2006) 16–28.
[26] M.R. Prairie, L.R. Evans, B.M. Stange, S.L. Marlinez, An investigation of TiO_2 photocatalysis for the treatment of water contaminated with metals and organic chemicals, Environ. Sci. Technol. 27 (1993) 1776–1782.
[27] G. Lente, J.H. Espenson, Photoreduction of 2,6-dichloroquinone in aqueous solution: use of a diode array spectrophotometer concurrently to drive and detect a photochemical reaction, J. Photochem. Photobiol. A 163 (2004) 249–258.
[28] A. Sorokin, S. De Suzzoni-Dezard, D. Poullain, J.P. Noël, B. Meunier, CO_2 as the ultimate degradation product in the H_2O_2 oxidation of 2,4,6-trichlorophenol catalyzed by iron tetrasulfophthalocyanine, J. Am. Chem. Soc. 118 (1996) 7410–7411.
[29] S.S. Gupta, M. Stadler, C.A. Noser, A. Ghosh, B. Steinhoff, D. Lenoir, C.P. Horwitz, K.W. Schramm, T.J. Collins, Rapid total destruction of chlorophenols by activated hydrogen peroxide, Science 296 (2002) 326–328.
[30] A. Sorokin, J.L. Séris, B. Meunier, Efficient oxidative dechlorination and aromatic ring cleavage of chlorinated phenols catalyzed by iron sulfophthalocyanine, Science 268 (1995) 1163–1166.
[31] E.B. Rinker, S.S. Ashour, M.C. Johnson, G.J. Kott, R.G. Rinker, O.C. Sandall, Kinetics of the aqueous-phase reaction between ozone and 2,4,6-trichlorophenol, AIChE J. 45 (1999) 1802–1807.